Research Papers

GREENSUSMATER

Greensusmater
Vol. 1, No. 1, 2026
https://doi.org/10.62755/gsm.2026.01

Check for updates

Influence of Nb dopant concentration on the structural properties and photocatalytic performances of hydrothermally synthesized ZnO for multi-pollutant degradation

Quratul Aini[1,*], Carenina Isabel Suwono Putri[1], Rima Nurfitria[1], Istiara Rizqillah Hanifah[1]

[1] *Department of Materials Engineering, Faculty of Industrial Technology, Institut Teknologi Sumatera, Terusan Ryacudu, Way Hui, Jati Agung, Lampung Selatan 35365, Indonesia*

Corresponding author: quratul.aini@mt.itera.ac.id

ARTICLE HISTORY: Received: February 18, 2026 | Revised: April 21, 2026 | Accepted: April 23, 2026

ABSTRACT

The development of effective photocatalysts for multi-pollutant wastewater remediation remains a significant environmental concern. In this study, Nb-doped ZnO photocatalysts with different Nb concentrations (0-6%) were synthesized using a hydrothermal process to systematically examine the influence of dopant concentration on materials characteristics and photocatalytic performance. According to X-ray diffraction analysis Nb incorporation preserved the hexagonal wurtzite ZnO structure with only slight lattice parameter changes, suggesting limited substitutional doping. Morphological observations showed that moderate Nb doping slightly enhanced particle structure and reduced agglomeration. The photocatalytic activity was evaluated through the degradation of ciprofloxacin (CIP) and methylene blue (MB) under UV irradiation, both in single and mixed pollutant systems. In single systems, the catalysts achieved high degradation efficiencies of up to 93.09% for CIP and 92.03% for MB after 120 min. In the mixed system, the efficiencies slightly decreased due to competitive interactions, reaching up to 87.57% (CIP) and 84.08% (MB). Kinetic analysis indicates pseudo-first-order behavior, with apparent rate constants (k) of approximately 0.0218 min^{-1} (CIP) and 0.0199 min^{-1} (MB) for the optimally doped Nb4-ZnO sample, which are comparable to those of pristine ZnO. The findings highlight the critical role of dopant concentration in tailoring structural and electronic properties, providing valuable insights into Nb-dopant optimization strategies for efficient multi-pollutant photocatalytic wastewater remediation.

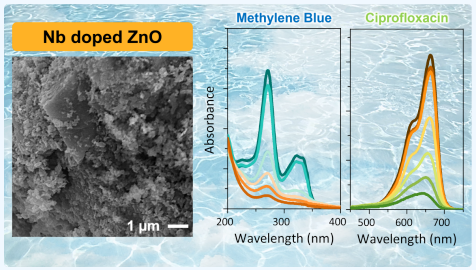

Keywords: *Wastewater treatment; Dopant optimization; Nb-doped ZnO; methylene blue; Ciprofloxacin*

1. INTRODUCTION

The rapid development of industrial activities is causing the continuous release of multi pollutants into aquatic environments, which causes great threats to both ecosystem and human health. In the pharmaceutical industry, ciprofloxacin (CIP) antibiotics are known as a micropollutant which exists in aquatic environments in the range of 150 µg/L to 21 mg/L [1,2]. In CIP, piperazinyl (-NH_2) and quinolone (-O-CH_3, -O-CHF_2) functional groups are present, which makes it hazardous to the aquatic ecosystem [3]. Another most found pollutant is methylene blue (MB), which is a frequently used dye in the textile and paper industries. MB exhibits high chemical stability and strong resistance to biodegradation, making it difficult to remove through conventional treatment methods [4,5]. These industries are among the major contributors to dye-containing effluents, with textile and leather sectors alone accounting for approximately 17-20% of global water pollution, as reported by the World Bank. MB exhibits high chemical stability and strong resistance to biodegradation, making it difficult to remove through conventional treatment methods [6,7]. The coexistence of such pharmaceuticals and dyes highlights the urgency of developing efficient and sustainable strategies for the remediation of multi-pollutant wastewater.

Several approaches have been explored for the treatment of MB- and CIP-contaminated water, including coagulation-flocculation, membrane separation, adsorption, and advanced oxidation processes (AOPs) [8,9,10,11]. Nevertheless, these conventional methods often exhibit limited efficiency in completely removing persistent pollutant molecules and may involve secondary pollution or high operational costs [9,10,11]. However, advanced oxidation processes have attracted increasing interest, among which photocatalytic oxidation stands out as an effective AOP due to its ability to generate highly reactive oxidative species, enabling the deep degradation and mineralization of the multi-pollutant components under light irradiation [8].

Semiconductor-based photocatalysis has emerged as a promising method for breaking down pollutants, as it is able to mineralize the toxic compounds under light exposure without producing harmful byproducts [1]. Among these materials, zinc oxide (ZnO) stands out as a widely researched photocatalyst due to its affordability, safety, high photosensitivity, and strong oxidation potential. Yet its broad band gap and quick recombination of light-induced electrons and holes greatly restrict its photocatalytic performance. Thus, simple and rational modification of ZnO is essential to overcome these intrinsic limitations and improve its photocatalytic performance [2,5,12,13].

Recently, elemental doping has been widely employed as an effective strategy to address the limitations of ZnO by

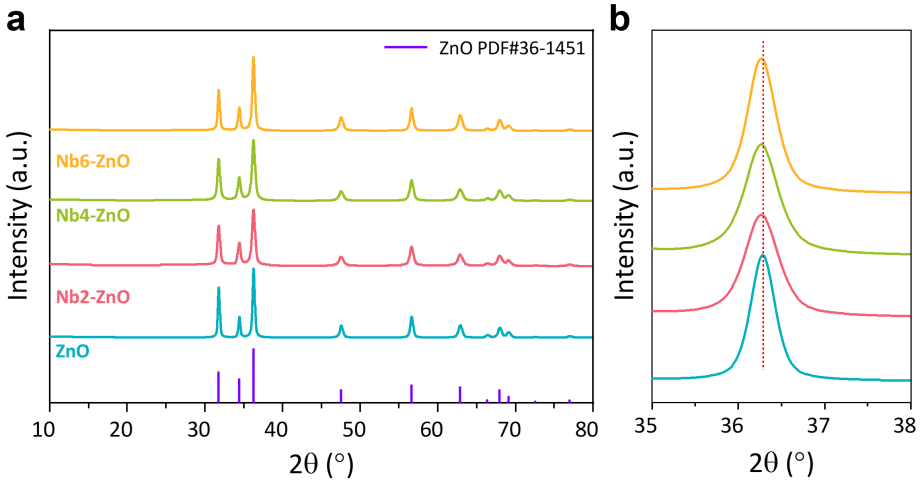

Figure 1. X-ray diffraction (XRD) patterns of niobium (Nb)-doped zinc oxide (ZnO). (a) Full XRD spectra showing pure ZnO and Nb-doped samples (Nb2-ZnO, Nb4-ZnO, Nb6-ZnO) compared with the standard ZnO reference pattern (PDF#36-1451). (b) Magnified view of the main diffraction peak showing peak shift with Nb doping concentration.

altering its electronic structure and defect sites [14,15,16,17]. Niobium (Nb) stands out as a dopant due to its higher valence state (Nb^{5+}) compared to Zn^{2+}, which creates donor levels and boosts charge carrier density [18,19]. Embedding Nb in the ZnO lattice should improve the crystal structure, optical traits, and charge dynamics, ultimately boosting photocatalysis. However, excessive dopant incorporation may also act as recombination traps, leading to a decline in photocatalytic activity. Therefore, tuning the concentration is crucial to enhance photocatalytic performance [13,18,19,20].

Hydrothermal synthesis provides a versatile and controllable approach in fabricating doped ZnO materials under relatively mild conditions with well-defined morphology, increased crystallinity, and uniform distribution of dopant particles [21]. Despite several previous studies on Nb-doped ZnO photocatalysts, a systematic study focusing on the role of Nb dopant concentration in tailoring the structural and photocatalytic properties of hydrothermally synthesized ZnO remains limited. In particular, the correlation between dopant concentration, structural evolution, and photocatalytic activity remains insufficiently understood.

Herein, Nb-doped ZnO nanoparticles were synthesized using the hydrothermal method. By varying the Nb concentrations, the changes of their structural and optical properties due to the Nb influences were comprehensively investigated. To demonstrate their potential for broad-spectrum pollutant removal, the as-synthesized photocatalysts were assessed through the photocatalytic degradation of multi-pollutant, including ciprofloxacin (CIP) and methylene blue (MB). A comprehensive analysis of the role of Nb dopant on structural characteristics and photocatalytic performance of ZnO provides valuable insights about dopant optimization strategies for achieving efficient multi-pollutant removal.

2. MATERIALS AND METHODS

2.1 Materials

Zinc nitrate hexahydrate ($Zn(NO_3)_2{\cdot}6H_2O$, 98%, Sigma-Aldrich) was used as the zinc precursor. Polyvinylpyrrolidone (PVP) and urea (Sigma-Aldrich) were employed as a surfactant and precipitating agent, respectively. Ammonium niobate(V) oxalate hydrate (99%, Sigma-Aldrich) was used as the Nb dopant source. Ciprofloxacin (CIP) and methylene blue served as multi-pollutant model for photocatalytic evaluation. All chemicals were used as received without further purification.

2.2 Synthesis of Nb-ZnO nanophotocatalysts

Nb-doped ZnO (Nb-ZnO) materials were synthesized via a hydrothermal method with Nb doping ratios of 0, 2, 4, and 6% (refer to molar ratio of Nb relative to Zn). For all samples, zinc nitrate hexahydrate ($Zn(NO_3)_2{\cdot}6H_2O$) was used as the Zn precursor with a constant mass of 2.380 g. Urea ($CO(NH_2)_2$) and polyvinylpyrrolidone (PVP, $(C_6H_9NO)_n$) were added as the precipitating agent and surfactant, respectively. Ammonium niobate(V) oxalate hydrate ($C_4H_4NNbO_9{\cdot}4H_2O$) served as the Nb dopant source, with masses of 0, 0.06, 0.12, and 0.18 g corresponding to Nb ratios of 0, 2, 4, and 6% (denoted as ZnO, Nb2-ZnO, Nb4-ZnO, and Nb6-ZnO). The ZnO precursor solution was prepared by dissolving $Zn(NO_3)_2{\cdot}6H_2O$, urea, and PVP in 35 mL of deionized water and stirring for 20 min until homogeneous. The Nb precursor was separately dissolved in 35 mL of deionized water and stirred for 20 min. The Nb-containing solution was then slowly added to the ZnO precursor solution according to the desired Nb ratio under continuous stirring to avoid agglomeration. The resulting mixture was transferred into a Teflon-lined autoclave and subjected to hydrothermal treatment at 175 °C for 24 h. After cooling, the product was collected by vacuum filtration, dried at 100 °C for 6 h, and calcined at 600 °C for 2 h with a heating rate of 3 °C min^{-1} to obtain Nb-ZnO nanophotocatalyst powder.

2.3 Materials characterization

The crystalline structure of the synthesized samples was analyzed using X-ray diffraction (XRD) on a Rigaku SmartLab SE Basic diffractometer equipped with Cu Kα radiation (λ = 1.5406 Å). The diffraction patterns were recorded over a 2θ range of 10° to 80° with a scanning rate of 2°/min. The average crystallite size was estimated using the Scherrer equation. The surface morphology and elemental composition of the samples were examined using scanning electron microscopy (SEM-EDS) on a JEOL JSM-6510 microscope.

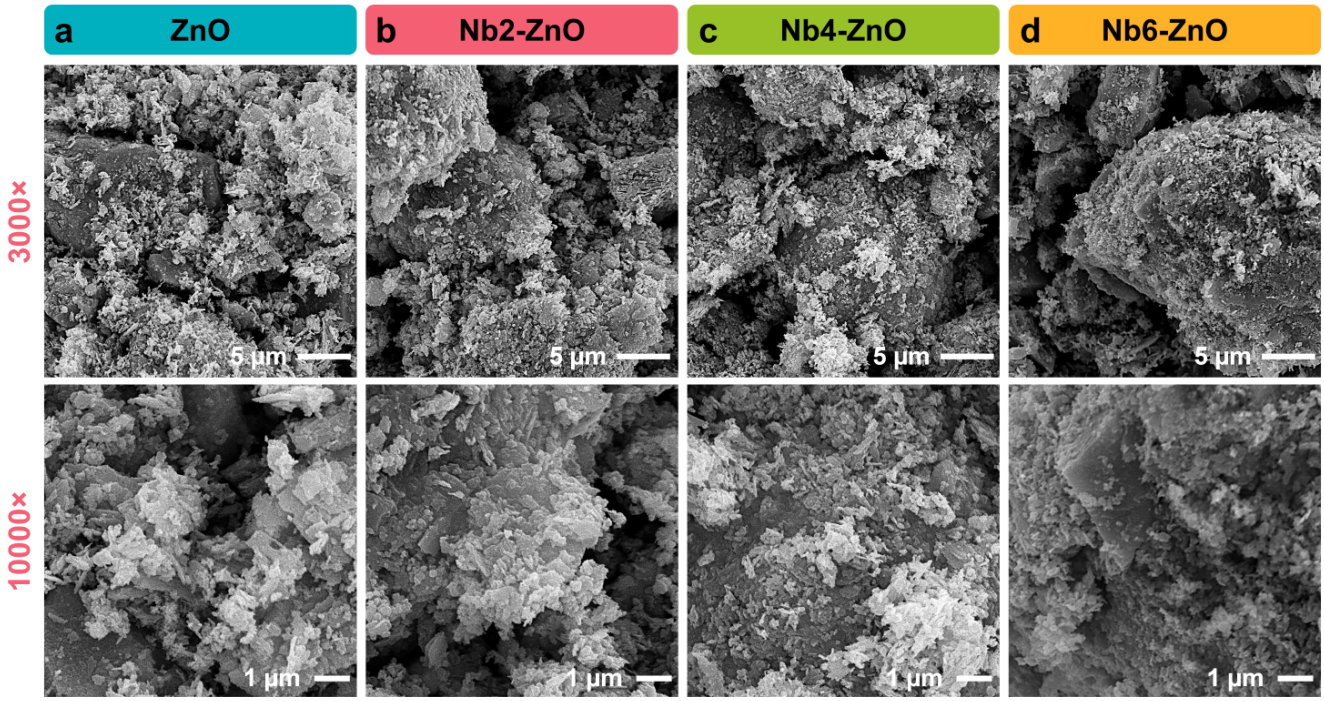

Figure 2. Scanning electron microscopy (SEM) images pure and niobium (Nb)-doped zinc oxide (ZnO) nanostructures. (a) Pure ZnO, (b) Nb2-ZnO, (c) Nb4-ZnO, and (d) Nb6-ZnO at two different magnifications (top row: 3000×, scale bar = 5 μm; bottom row: 10000×, scale bar = 1 μm) showing the morphological changes with increasing Nb doping concentration.

2.4 Photocatalytic dye degradation measurements

The photocatalytic performance of the synthesized Nb-doped ZnO samples was investigated by monitoring the degradation of Ciprofloxacin (CIP, an antibiotics), methylene blue (MB, a cationic dye) and a mix CIP-MB solution under UV light irradiation. In each experiment, 50 mg of photocatalyst was dispersed in 100 mL of an aqueous pollutant solution with an initial concentration of 5 mg L^{-1}. The suspension was continuously stirred during UV exposure to maintain uniform dispersion. Photocatalytic experiments were carried out using four 10 W Philips TUV lamps ($\lambda \approx 254$ nm) to provide uniform irradiation. At 30 min intervals, 3.5 mL aliquots were collected and immediately filtered using syringe filters to remove catalyst particles. The residual pollutant concentration was determined by measuring the absorbance of the filtrate at 664 nm using a Shimadzu UV-1280 UV-Vis spectrophotometer.

3. RESULTS AND DISCUSSION

The X-ray diffraction (XRD) patterns presented in Figure 1a confirm that all synthesized samples exhibit a hexagonal wurtzite crystal structure corresponding to zinc oxide (ZnO), as evidenced by the excellent match with the standard reference pattern (PDF#36-1451). No additional peaks associated with crystalline niobium (Nb) oxide phases or other impurities were detected across all doping concentrations (Nb2-ZnO, Nb4-ZnO, and Nb6-ZnO), indicating that the wurtzite structure is preserved regardless of Nb content.

The magnified view of the (101) diffraction peak in Figure 1b reveals a small shift toward lower 2θ values upon the introduction of Nb. The pure ZnO sample exhibits the (101) peak at $2\theta = 36.287°$, while the Nb-containing samples show peak positions at 36.259°, 36.260°, and 36.261° for Nb2-ZnO, Nb4-ZnO, and Nb6-ZnO, respectively. According to Bragg's law, a shift to lower 2θ corresponds to a slight increase in interplanar d-spacing. However, the nearly identical peak positions across all three Nb concentrations despite a threefold increase in Nb content from Nb2 to Nb6, suggest that this shift does not follow a systematic, concentration-dependent trend as would be expected for progressive substitutional doping. This behavior may indicate that only a highly limited amount of Nb is incorporated into the ZnO lattice, with a significant fraction of Nb is not incorporated into ZnO possibly residing as amorphous niobium oxide on the surface or segregated at grain boundaries, which would remain undetectable by XRD. The significant charge mismatch between Nb^{5+} and Zn^{2+} further supports this interpretation, as direct substitution would require extensive charge compensation mechanisms, making large-scale incorporation energetically unfavorable.

Table 1. Crystallographic parameters and reliability factors of pure and niobium (Nb)-doped zinc oxide (ZnO) samples obtained from Rietveld refinement of X-ray diffraction (XRD) data.

Sample	ZnO crystallographic parameters		Reliability factors			
	a (Å)	c (Å)	R_{wp}	R_{exp}	χ^2	GoF
ZnO	0.325062	0.520856	9.09	8.16	1.2409	1.1140
Nb2-ZnO	0.325078	0.520964	8.91	7.83	1.2949	1.1379
Nb4-ZnO	0.325094	0.521021	9.19	7.89	1.3567	1.1648
Nb6-ZnO	0.325075	0.520908	9.31	8.29	1.2612	1.1230

The crystallographic parameters obtained from Rietveld refinement, summarized in Table 1, show only minor varia-

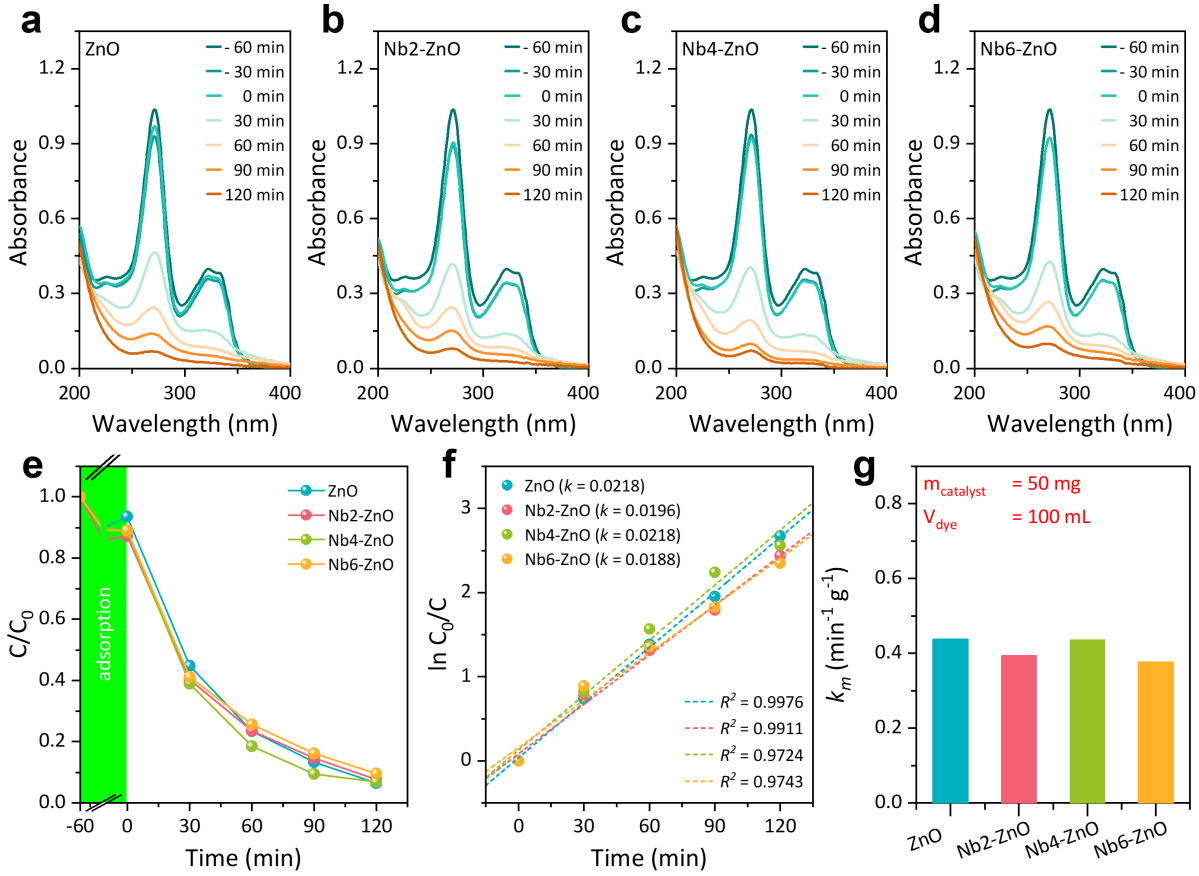

Figure 3. Time-dependent UV-Vis absorbance spectra of ciprofloxacin (CIP) recorded under UV irradiation in the presence of (a) ZnO, (b) Nb2-ZnO, (c) Nb4-ZnO, and (d) Nb6-ZnO. The photocatalytic degradation performance of ZnO and Nb-doped ZnO samples, (e) degradation profiles of CIP concentration over time, (f) pseudo-first-order kinetic fitting plots, and (g) kinetic rate constants normalized to mass of catalysts.

tions in the a and c lattice parameters across all samples, consistent with the limited peak shift observed. The goodness-of-fit (GoF) values close to unity and low chi-square (χ^2) values across all samples confirm the reliability of the refined structural data and the adequacy of the hexagonal wurtzite model for describing both pure and Nb-containing ZnO.

The SEM images (Figure 2) show that Nb doping clearly affects the shape of ZnO particles. Undoped ZnO with high surface energy is characterized by large, irregular agglomerates made of closely spaced particles, as seen in pristine ZnO (Figure 2a) [14]. The introduction of Nb at low to moderate concentrations (Nb2-ZnO and Nb4-ZnO) stimulated the loss of agglomerates and generated the homogeneous structure as shown in Figure 2b-c, while the particle surfaces seem finer and more porous. Furthermore, Nb4-ZnO in Figure 2d shows the relatively more uniform morphology shape, showing the Nb inclusion efficiently restricts grain development and promotes the production of smaller particles. This morphological refinement shows a strong relationship between dopant concentration, and microstructural alterations.

The morphology collapses at greater Nb concentration (Nb6-ZnO), as shown by the production of irregular and dense agglomerates. Lattice distortion or dopant segregation is caused by excessive Nb incorporation, which surpasses the solubility limit of Nb in the ZnO lattice. These actions promote particle coalescence and raise surface energy, which causes re-agglomeration. These findings imply that there may be an ideal concentration of Nb at which grain development is successfully suppressed without causing phase separation or structural instability. As a result, Nb4-ZnO is the most advantageous composition for attaining improved surface properties and controlled microstructure, both of which are essential for photocatalysis applications. The reduction agglomeration in Nb4-ZnO promote high surface area, may contribute to improved accessibility of active sites, although photocatalytic performance is also strongly governed by electronic effects [22].

Figure 3 depicts the degradation behavior of Ciprofloxacin (CIP) photocatalytic over pure ZnO and Nb-doped ZnO catalysts under UV irradiation. The typical UV-Vis absorption peaks of CIP progressively diminish with longer irradiation times, as illustrated in Figures 3a-d, demonstrating the efficient photocatalytic breakdown of CIP. Compared to pristine ZnO, the Nb-doped samples exhibit a comparative reduction in absorbance intensity, suggesting a relatively low enhancement in photocatalytic activity upon Nb incorporation. The temporal evolution of CIP concentration (C/C_0), presented in Figure 3e, shows a continuous decline for all samples throughout the irradiation period. Although Nb-doped ZnO demonstrates comparable or slightly improved degradation behavior relative to undoped ZnO, the differences among the samples are not pronounced.

Figure 3f displays the kinetic analysis of the degradation

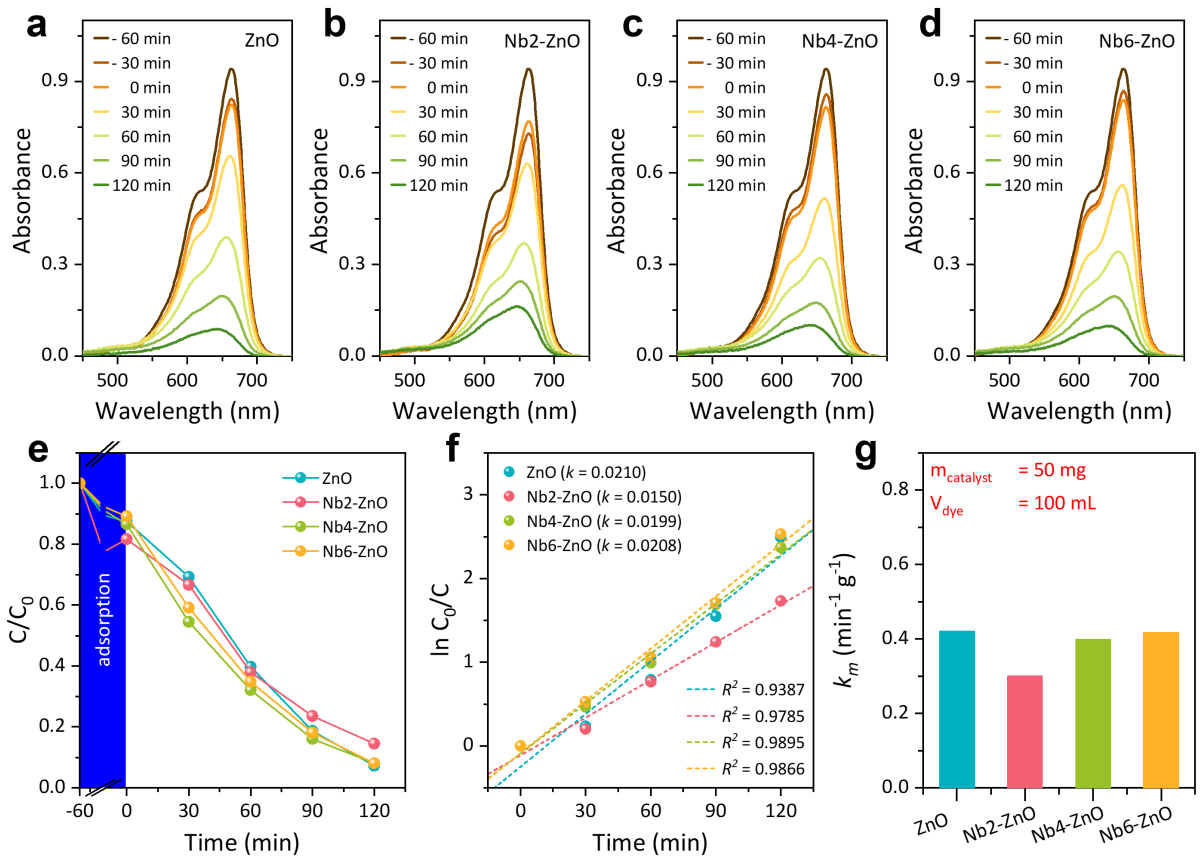

Figure 4. Time-dependent UV-Vis absorbance spectra of methylene blue (MB) recorded under UV irradiation using (a) ZnO, (b) Nb2-ZnO, (c) Nb4-ZnO, and (d) Nb6-ZnO photocatalyst. The photocatalytic degradation performance of ZnO and Nb-doped ZnO samples, (e) the profiles of concentration decay, (f) pseudo-first-order kinetic analysis, and (g) mass-normalized kinetic rate constants.

process. According to the linear fitting of $\ln(C_0/C)$ against irradiation time, pseudo-first-order reaction kinetics govern CIP degradation across all catalysts [18]. For detail comparison, Figure 3g summarizes the corresponding apparent rate constants normalized to catalyst mass. ZnO and Nb4-ZnO exhibit comparable rate constants (k=0.0218 min^{-1} and k=0.0218 min^{-1}, respectively), while Nb2-ZnO and Nb6-ZnO show slightly lower values (k=0.0196 min^{-1} and k=0.0196 min^{-1}, respectively). The apparent rate constants (k) for CIP degradation are relatively close for all samples, with only minor differences observed between Nb4-ZnO and Nb6-ZnO. This indicates that the effect of Nb doping on the intrinsic reaction kinetics is limited, and the observed variations are not practically significant. Furthermore, the corresponding efficiencies were 93.09%, 91.26%, 92.27%, and 90.44% for ZnO, Nb4-ZnO, Nb2-ZnO and Nb6-ZnO, respectively. This suggests that Nb doping does not significantly enhance the intrinsic degradation rate of CIP but helps maintain comparable activity at an optimal doping level. The absence of substantial improvement may be attributed to the limited incorporation of Nb into the ZnO lattice, as indicated by XRD analysis. Additionally, the reduction of performance in heavy Nb doping causes a modest decrease in activity, which is probably caused by the partial blockage of active sites or the creation of recombination centres.

Figures 4a-d present the time-dependent UV-Vis absorption spectra of methylene blue (MB) during UV irradiation in the presence of pristine ZnO and Nb-doped ZnO photocatalysts. The characteristic MB absorption peak at around ~664 nm steadily decreases with irradiation duration for all samples, suggesting efficient photocatalytic breakdown rather than mere adsorption. In contrast to pristine ZnO [4,5], Nb-doped ZnO exhibits a faster fall in absorbance intensity than pristine ZnO, proving the Nb incorporation enhances the photocatalytic activity of ZnO toward MB degradation. The concentration declines profiles of all catalysts (Figure 4e) further support this tendency by demonstrating continued MB degradation under UV light after the first dark adsorption phase. The most noticeable degrading efficiency among the doped samples is shown by Nb4-ZnO and Nb6-ZnO, which achieve lower residual MB concentrations in the same duration of irradiation time. This enhancement can be associated to the substitution of Nb^{5+} for Zn^{2+}, since it adds more donor states, raises the density of charge carriers, and facilitates the more effective separation of photogenerated electron-hole pairs. In contrast, Nb2-ZnO exhibits noticeably poorer performance, indicating the advantageous electrical change is limited by inadequate dopant concentration [19,20,23].

To quantitatively analyze the degradation kinetics, pseudo-first-order kinetic fitting was applied (Figure 4f). The high correlation values ($R^2 > 0.97$) and a linear relationship between $\ln(C_0/C)$ and irradiation duration, MB degradation is confirmed to follow pseudo-first-order kinetics for all samples [4,18]. The calculated apparent rate constants (k) are

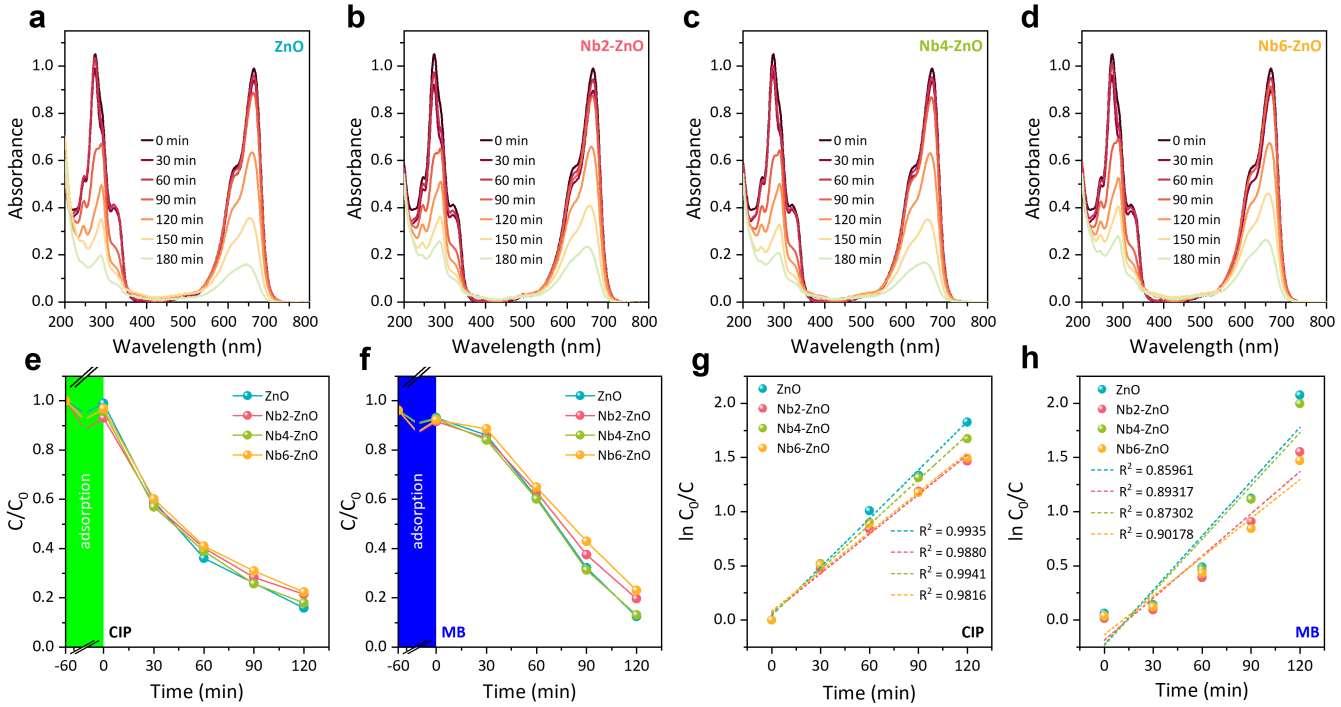

Figure 5. Photocatalytic degradation of mixed ciprofloxacin (CIP) and methylene blue (MB) solution using pure and niobium (Nb)-doped zinc oxide (ZnO). UV-Vis absorption spectra at different irradiation times for (a) ZnO, (b) Nb2-ZnO, (c) Nb4-ZnO, and (d) Nb6-ZnO. (e, f) Degradation profiles (C/C_0) of CIP and MB, respectively. (g, h) Pseudo-first-order kinetic fitting with corresponding R^2 values for CIP and MB, respectively.

0.0210, 0.0150, 0.0199, and 0.0208 min^{-1} for ZnO, Nb2-ZnO, Nb4-ZnO, and Nb6-ZnO, respectively. These values indicate that the photocatalytic activities of Nb4-ZnO and Nb6-ZnO are comparable to that of pristine ZnO, while Nb2-ZnO exhibits a noticeably lower rate constant. The degradation efficiencies for MB were 91.74%, 82.29%, 90.67%, and 92.03% for ZnO, Nb2-ZnO, Nb4-ZnO, and Nb6-ZnO, respectively. This suggests that Nb doping does not lead to a significant enhancement in the intrinsic degradation rate of MB, and that the effect of dopant concentration is relatively moderate. The absence of a clear improvement may be attributed to the limited incorporation of Nb into the ZnO lattice, as suggested by XRD and EDS analyses, as well as the possible formation of defect states that can act as recombination centers at non-optimal doping levels. By excluding the effects of catalyst loading, the mass-normalized kinetic rate constants (Figure 4g) further support these findings. ZnO, Nb4-ZnO, and Nb6-ZnO exhibit comparable values, while Nb2-ZnO remains the lowest. These results indicate that Nb doping does not produce a pronounced increase in photocatalytic performance toward MB degradation, but rather maintains comparable activity within an optimal doping range.

Figure 5 illustrates how pure ZnO and Nb-doped ZnO catalysts photocatalytically degrade mixed CIP-MB solutions when exposed to irradiation. The typical absorption peaks of CIP and MB gradually diminish with increasing irradiation time, as demonstrated by the UV-Vis absorption spectra (Figure 5a-d), confirming the progressive destruction of both pollutants. The peak intensity decreases in all samples, with Nb4-ZnO showing a marginally greater reduction, suggesting a slight improvement in photocatalytic performance. This slightly enhanced performance of Nb4-ZnO for the mix CIP-MB pollutant is further demonstrated by the degradation patterns (C/C_0) shown in Figure 5e-f. All catalysts exhibit adsorption during the dark equilibrium phase, but when exposed to light, photocatalytic removal takes over. The sample with the lowest residual concentration after 120 minutes is Nb4-ZnO, indicating that catalytic performance is maximized by modest Nb incorporation. On the other hand, performance is marginally reduced by excessive doping (Nb6-ZnO), most likely because of the increased defects sites formation which serving as charge recombination area.

After 120 min of irradiation, the degradation efficiencies for MB are 84.08%, 78.54%, 82.04%, and 77.57%, while for CIP they are 87.57%, 80.29%, 86.99%, and 76.99% for ZnO, Nb2-ZnO, Nb4-ZnO, and Nb6-ZnO, respectively. These results indicate that ZnO and Nb4-ZnO exhibit relatively higher degradation performance in the mixed system, whereas Nb2-ZnO and Nb6-ZnO show slightly reduced efficiencies. The overall decrease in degradation efficiency compared to single-pollutant systems can be attributed to competitive interactions between CIP and MB for active sites and reactive species. Under the applied conditions, the degradation of both CIP and MB follows pseudo-first-order reaction behaviour, as confirmed by the pseudo-first-order kinetic plots (Figure 5g-h), which show good linear correlation and high R^2 values (usually >0.85) [18]. Nb4-ZnO exhibits the highest apparent rate constant for both contaminants among all samples, indicating its exceptional photocatalytic effectiveness.

Compared to those systems in Table 2, Nb-doped ZnO in this study exhibits comparable photocatalytic performance rather than a significant enhancement, which may be associated with the limited incorporation of Nb into the ZnO lattice. Nevertheless, the results demonstrate that Nb doping can maintain stable activity, particularly under mixed-pollutant conditions, emphasizing its potential for practical wastewater

Table 2. Comparison of photocatalytic performance of pure metal-doped ZnO samples from previous studies.

Dopant	Pollutants	Performance	ref
Nb	CIP-MB	k=0.0218 min^{-1} at 120 min irradiation (CIP/single pollutant) k=0.0199 min^{-1} at 120 min irradiation (MB/single pollutant)	This work
Cu	MB	k=0.0274 min^{-1} at 120 min irradiation (MB/single pollutant	[24]
Ni	MB	k=0.0081 min^{-1} at 120 min irradiation (MB/single pollutant	[24]
Co	MB	k=0.0058 min^{-1} at 120 min irradiation (MB/single pollutant	[24]
Fe	MB	k=0.0036 min^{-1} at 120 min irradiation (MB/single pollutant	[24]
Mn	MB	k=0.0163 min^{-1} at 120 min irradiation (MB/single pollutant	[24]

treatment applications.

4. CONCLUSION

This study successfully synthesized Nb-doped ZnO photocatalysts via a simple hydrothermal method and systematically investigate the dopant concentration contributions on the structural evolution and multi-pollutant photocatalytic performance. Following Nb incorporation, the synthesized photocatalyst retained the hexagonal wurtzite structure of ZnO with decreased agglomeration and more homogeneous microstructure. Photocatalytic evaluation demonstrates that all samples exhibit high degradation efficiencies in single-pollutant systems, reaching up to ~92% for MB and ~93% for CIP after 120 min. In the mixed CIP-MB system, the efficiencies decrease slightly to ~82-84% for MB and ~86-87% for CIP for the best-performing samples, due to competitive interactions between pollutants. Kinetic analysis confirms pseudo-first-order behavior, with comparable apparent rate constants among the samples (e.g., k ≈ 0.0199 min^{-1} for MB and 0.0218 min^{-1} for CIP for Nb4-ZnO), indicating that Nb doping provides only moderate influence on intrinsic reaction rates. Among the studied samples, Nb4-ZnO demonstrates relatively stable and balanced photocatalytic performance, particularly under multi-pollutant conditions. Overall, these findings highlight the importance of Nb dopant optimization in achieving stable and effective ZnO-based photocatalysts for wastewater treatment applications, especially in complex pollutant environments.

ACKNOWLEDGMENTS

This study receives no funding.

DATA AVAILABILITY STATEMENT

The datasets generated during and/or analyzed during the current study are available from the corresponding author on reasonable request.

CONFLICT OF INTEREST

The authors declare that there are no conflicts of interest.

AUTHOR CONTRIBUTIONS

Quratul Aini: Conceptualization, methodology, investigation, data curation, formal analysis, writing-original draft, and supervision. **Carenina Isabel Suwono Putri** and **Rima Nurfitria**: Investigation, experimental work, data curation, and visualization. **Istiara Rizqillah Hanifah**: Methodology support, validation, and writing-review & editing.

REFERENCES

[1] Oliveira JA, Reis MO, Pires MS, Ruotolo LAM, Ramalho TC, Oliveira CR, Lacerda LCT, Nogueira FGE. Zn-doped Nb2O5 photocatalysts driven by visible-light: An experimental and theoretical study. *Materials Chemistry and Physics*. 2019;228:160-167. doi:10.1016/j.matchemphys.2019.02.062.

[2] Thuan DVan, Nguyen TBH, Pham TH, Kim J, Chu TTHien, Nguyen MV, Nguyen KD, Al-Onazi WA, Elshikh MS. Photodegradation of ciprofloxacin antibiotic in water by using ZnO-doped g-C(3)N(4) photocatalyst. *Chemosphere*. 2022;308(Pt):136408. doi:10.1016/j.chemosphere.2022.136408.

[3] Amir M, Fazal T, Iqbal J, Din AA, Ahmed A, Ali A, Razzaq A, Ali Z, Rehman MSU, Park Y-K. Integrated adsorptive and photocatalytic degradation of pharmaceutical micropollutant, ciprofloxacin employing biochar-ZnO composite photocatalysts. *Journal of Industrial and Engineering Chemistry*. 2022;115:171-182. doi:10.1016/j.jiec.2022.07.050.

[4] Ameen S, Fatima R, Kadhem AA, Abbas T, Khan MA, Abbas A, Hussain I, Bano N, Rad ZFaraji, Bilal ASS. Enhanced photocatalytic degradation of methylene blue using aluminum and cerium co-doped ZnO nanocomposite. *International Journal of Environmental Science and Technology*. 2025;22(16):16549-16558. doi:10.1007/s13762-025-06683-z.

[5] Habibollahi Z, Peyravi M, Khalili S, Jahanshahi M. ZnO-based ternary nanocomposite for decolorization of methylene blue by photocatalytic dynamic membrane. *Materials Today Chemistry*. 2022;23. doi:10.1016/j.mtchem.2021.100748.

[6] Khan SA, Arshad Z, Shahid S, Arshad I, Rizwan K, Sher M, Fatima U. Synthesis of TiO2/Graphene oxide nanocomposites for their enhanced photocatalytic activity against methylene blue dye and ciprofloxacin. *Composites Part B: Engineering*. 2019;175:107120. doi:10.1016/j.compositesb.2019.107120.

[7] Yang F, Zhang J, Lin T, Ke L, Huang L, Deng S-P, Zhang J, Tan S, Xiong Y, Lu M. Fabrication of waste paper/graphene oxide three-dimensional aerogel with dual adsorption capacity toward methylene blue and ciprofloxacin. *Journal of the Iranian Chemical Society*. 2023;20(4):801-816. doi:10.1007/s13738-022-02714-5.

[8] Chen Z, Wei W, Chen H, Ni B-J. Recent advances in waste-derived functional materials for wastewater remediation. *Eco-Environment & Health*. 2022;1(2):86-104. doi:10.1016/j.eehl.2022.05.001.

[9] Fitri A, Prasetya B, Aini Q, Ikhsan F, Aflaha R, Triyana K, Taher T, Arif MF, Rianjanu A. Enhanced methylene blue adsorption capacity of 3D-printed zeolite/glycerol (3D-Ze/Gy) by sintering temperature optimization. *Next Materials*. 2025;9. doi:10.1016/j.nxmate.2025.101069.

[10] Phasa A, Aini Q, Siregar MY, Sabilla S, Triyadi D, Aflaha R, Khan MGI, Nurfani E. Photocatalytic degradations of organic pollutants in wastewater using hydrothermally grown ZnO nanoparticles. *Greensusmater*. 2024;1(2):39-43. doi:10.62755/greensusmater.2024.1.2.39-43.

[11] Rianjanu A, Aini Q, Hanif R, Tambun SA, Triyadi D, Aflaha R, Yulianto N, Yudistira HT, Herbani Y, Taher T, Wasisto HS. Influence of temperature and reaction time on photocatalytic performance of BaTiO3 nanoparticles for organic pollutant degradation in aqueous environment. *Surfaces and Interfaces*. 2025;70. doi:10.1016/j.surfin.2025.106875.

[12] Pantoja-Espinoza JC, DelaCruz-Alderete GA, Paraguay-Delgado F. Photocatalytic Degradation of Methylene Blue Dye

with g-C3N4/ZnO Nanocomposite Materials Using Visible Light. *Catalysts*. 2025;15(9). doi:10.3390/catal15090851.

[13] Silva JMP, Julião RS, Nicácio TCN, Melo MCN, Santos RM, Bomio MRD, Motta FV. A study of Nb-doped ZnO ceramic and its enhanced solar photocatalysis, photoluminescence and antimicrobial properties. *Journal of Alloys and Compounds*. 2024;985. doi:10.1016/j.jallcom.2024.173978.

[14] Kohzadi S, Maleki A, Bundschuh M, Vahabzadeh Z, Johari SA, Rezaee R, Shahmoradi B, Marzban N, Amini N. Doping zinc oxide (ZnO) nanoparticles with molybdenum boosts photocatalytic degradation of Rhodamine b (RhB): Particle characterization, degradation kinetics and aquatic toxicity testing. *Journal of Molecular Liquids*. 2023;385. doi:10.1016/j.molliq.2023.122412.

[15] Alharshan GA, Aboraia AM, Uosif MAM, Sharaf IM, Shaaban ER, Saad M, Almohiy H, Elsenety MM. Optical Band Gap Tuning, DFT Understandings, and Photocatalysis Performance of ZnO Nanoparticle-Doped Fe Compounds. *Materials*. 2023;16(7). doi:10.3390/ma16072676.

[16] Muhammed A, Asere TG, Diriba TF. Photocatalytic and Antimicrobial Properties of ZnO and Mg-Doped ZnO Nanoparticles Synthesized Using Lupinus albus Leaf Extract. *ACS Omega*. 2024;9(2):2480-2490. doi:10.1021/acsomega.3c07093.

[17] Sivakumar S, Robinson Y, Mala NA. Studies on photocatalytic performance and supercapacitor applications of undoped and Cu-doped ZnO nanoparticles. *Applied Surface Science Advances*. 2022;12. doi:10.1016/j.apsadv.2022.100344.

[18] Nguyen THA, Le VT, Doan V-D, Tran AV, Nguyen VC, Nguyen A-T, Vasseghian Y. Green synthesis of Nb-doped ZnO nanocomposite for photocatalytic degradation of tetracycline antibiotic under visible light. *Materials Letters*. 2022;308. doi:10.1016/j.matlet.2021.131129.

[19] Ikram M, Shahid H, Haider J, Haider A, Naz S, Ul-Hamid A, Shahzadi I, Naz M, Nabgan W, Ali S. Expression of Concern for "Nb/Starch-Doped ZnO Nanostructures for Polluted Water Treatment and Antimicrobial Applications: Molecular Docking Analysis". *ACS Omega*. 2025;10(48):59999. doi:10.1021/acsomega.5c11085.

[20] Jusoh Y. Carrier Injection Mechanism of Nb-Doped ZnO Thin Films in Light Emission Properties. *PrzeglĄd Elektrotechniczny*. 2024;1(11):96-100. doi:10.15199/48.2024.11.17.

[21] Khan MGI, Nurfitria R, Anggraini T, Aini Q, Hanifah IR, Nurfani E, Aflaha R, Triyana K, Taher T, Rianjanu A. Hydrothermal synthesis of CeO2/ZnO heterojunctions for effective photocatalytic degradation of organic pollutants. *Materials Science and Engineering: B*. 2025;322. doi:10.1016/j.mseb.2025.118630.

[22] Ganguli AK, Kunde GB, Raza W, Kumar S, Yadav P. Assessment of Performance of Photocatalytic Nanostructured Materials with Varied Morphology Based on Reaction Conditions. *Molecules*. 2022;27(22). doi:10.3390/molecules27227778.

[23] Moraes NPde, Santos GSdos, Neves GC, Valim RB, Rocha RdaSilva, Landers R, Silva MLCaetanoPintoda, Rodrigues LA. Development of Nb2O5-doped ZnO/Carbon xerogel photocatalyst for the photodegradation of 4-chlorophenol. *Optik*. 2020;219. doi:10.1016/j.ijleo.2020.165238.

[24] Qi K, Xing X, Zada A, Li M, Wang Q, Liu S-y, Lin H, Wang G. Transition metal doped ZnO nanoparticles with enhanced photocatalytic and antibacterial performances: Experimental and DFT studies. *Ceramics International*. 2020;46(2):1494-1502. doi:10.1016/j.ceramint.2019.09.116.

